


Intrinsic Pink-Noise Multidecadal Global Climate Dynamics ModeWoosok Moon,^{1,2} Sahil Agarwal,³ and J. S. Wettlaufer^{3,2,4}¹*Department of Mathematics, Stockholm University, 106 91 Stockholm, Sweden*²*Nordita, Royal Institute of Technology and Stockholm University, SE-10691 Stockholm, Sweden*³*Yale University, New Haven, Connecticut 06520-8109, USA*⁴*Mathematical Institute, University of Oxford, Oxford OX2 6GG, United Kingdom* (Received 2 February 2018; revised manuscript received 2 April 2018; published 4 September 2018)

Understanding multidecadal variability is an essential goal of climate dynamics. For example, the recent phenomenon referred to as the “global warming hiatus” may reflect a coupling to an intrinsic, preindustrial, multidecadal variability process. Here, using a multifractal time-series method, we demonstrate that 42 data sets of 79 proxies with global coverage exhibit pink-noise characteristics on multidecadal timescales. To quantify the persistence of this behavior, we examine high-resolution ice core and speleothem data to find pink noise in both pre- and postindustrial periods. We examine the spatial structure with an empirical orthogonal function analysis of the monthly averaged surface temperature from 1901 to 2012. The first mode clearly shows the distribution of ocean heat flux sinks located in the eastern Pacific and the Southern Ocean and has pink-noise characteristics on a multidecadal timescale. We hypothesize that this pink-noise multidecadal spatial mode may resonate with externally driven greenhouse gas forcing, driving large-scale climate processes.

DOI: [10.1103/PhysRevLett.121.108701](https://doi.org/10.1103/PhysRevLett.121.108701)

A central question in contemporary climate science concerns the relative roles of natural climate variability and anthropogenic forcing. Indeed, understanding the detailed human effect on the global temperature is highly complex due to the nonlinear interactions of anthropogenic forcing with natural climate variability on multiple timescales, many of which transcend a typical human lifetime. The recent phenomenon referred to as the “global warming hiatus” [1–5] is a compelling example emphasizing the potential of such interactions. Understanding the coupling between natural multidecadal climate variability and anthropogenic forcing is a fundamental aspect of climate dynamics.

Here we describe a framework for characterizing the dynamics of natural global climate variability on multidecadal timescales [6–8]. There are many challenges associated with direct investigations of the physical and statistical characteristics of global observations on multiple timescales. First, the strong seasonal variability in observations, such as the surface air temperature, hinders the detection of long-term spatiotemporal correlations [9–11]. Moreover, there is a substantial land-ocean contrast in seasonal variability, making it difficult to extract the influence of climate variability on global scales. Second, the maximum length of the available station-based observations is only approximately 100 yr, which may be insufficient to statistically discern multidecadal variability. At the same time, nonlinear interactions between natural and anthropogenic contributions to the multidecadal variability found in these observations cannot be trivially disentangled. To overcome these obstacles, we analyze

the data in a manner that enables us to exclude the contributions of the strong seasonality in the station-based observations. We detect global multidecadal timescales corresponding to pink-noise dynamics, defined as having a power spectrum $S(f) \propto f^{-\beta}$, with frequency f and $\beta \approx 1$, also generally termed $1/f$ noise when $0 < \beta < 2$ (see, e.g., [12–17]). Furthermore, we analyze high-resolution proxy data spanning at least several hundred years to detect the footprint of these dynamics and to differentiate between anthropogenic forcing and natural climate variability.

We study the statistical characteristics of the decadal and multidecadal variability of Earth’s climate by analyzing the Goddard Institute for Space Studies (GISS) monthly averaged surface temperature data from 1901 to 2012 [18,19] and proxy data, such as $\delta^{18}\text{O}$ and $\delta^{13}\text{C}$, from ice cores and speleothems from 42 paleoclimate data sets (see Table 1 of Ref. [20]). To examine the temporal dynamics of the data, we use multifractal temporally weighted detrended fluctuation analysis (MFTW DFA) [11,23]. This methodology captures the statistical dynamics (e.g., white noise, red noise, and degree of correlation) on multiple timescales. The veracity of the approach has been demonstrated in various fields, such as the study of Arctic sea ice extent [11], sea ice velocity fields [24], and even the detection of exoplanets, in all cases solely using the data with no *a priori* modeling [25]. This approach produces a statistical measure called the fluctuation function $F_q(s)$, each moment of which q is assessed on multiple timescales s , as described in Refs. [11,20,23] in more detail. For intuition, one can think of the expectation value of $F_q(s)$

as the weighted sum of the autocorrelation function (see, e.g., [26]). The dominant timescales in a system are those where $F_q(s)$ versus s changes slope and the individual slopes are associated with the statistical dynamics of a system.

First, we analyze the GISS data set by employing a new stochastic dynamical method of time-series analysis that was shown to capture the seasonal variability in monthly averaged temperature data from decadal to 133 yr [27]. This method centers on a periodic nonautonomous stochastic model for the observed deviation in the surface heat flux, $x(t)$, given by $\dot{x} = a(t)x + N(t)\xi(t) + d(\tau)$, where $a(t)$ and $N(t)$ are periodic functions with annual periodicity, $\xi(t)$ is stochastic noise, and $d(\tau)$ represents decadal forcing. Thus, the first two terms in the model explain the seasonal variability, and the last term $d(\tau)$ captures the transseasonal variability. The approach provides analytical expressions for $a(t)$, $N(t)$, and $d(\tau)$ and reproduces the observed monthly statistics (Fig. 1 of Ref. [27]).

Second, we employ MFTW DFA to analyze the annual time series for each latitude-longitude pair from the GISS data set. A dominant signal at all locations is the presence of pink-noise behavior ($\beta \approx 1$) on multidecadal timescales. Pink noise, often referred to as “ubiquitous noise” (see, e.g., [12–17]), is observed in a wide range of systems, such as earthquakes, stellar luminosity, electronics, and climate on a variety of timescales (see, e.g., [14]). We quantify the spatial structure of this statistical behavior by showing the timescales on a global map; Fig. 1 shows the shortest timescale (in years) at which pink-noise behavior appears in the data. Latitude-longitude pairs that do not exhibit such behavior are shown in red, while points where no data were present are left blank. Timescales greater than about 60 yr are constrained by the finite length of the data set. Thus, the colors in Fig. 1 have two interpretations: pink noise from 1 to 60 yr but no pink noise for longer times. Because both $d(\tau)$ and the annual averaging of the data represent different forms of temporal filtering, they exhibit similar timescales for the global appearance of pink-noise behavior, hence we find quantitative but not qualitative differences [20]. However, the value of using $d(\tau)$ is that it embodies the effects of seasonal stability and noise on annual and longer timescales. The pointwise values of $d(\tau)$ in the GISS data set exhibit pink-noise characteristics on decadal and multidecadal timescales nearly everywhere on the globe. Dominant global climate variability phenomena such as the El Niño–Southern Oscillation (ENSO) immediately emerge from this analysis. The ENSO has been studied extensively and shown to influence global climate on timescales ranging from interannual to multidecadal through atmospheric and oceanic teleconnections (see, e.g., [28]). This phenomenon has also been related to global rainfall, a driver of global natural climate variability, which is a response to the regional amount of precipitation and

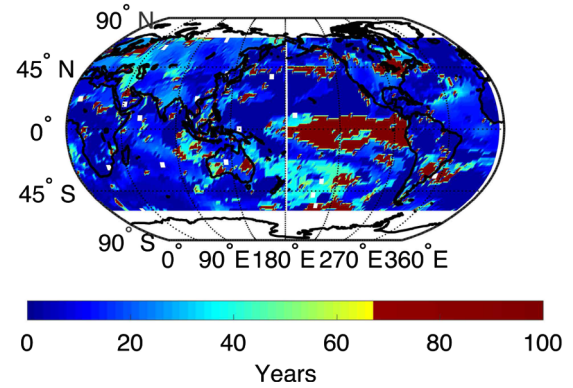


FIG. 1. Spatial distribution of the shortest timescale (in years) at which pink-noise behavior appears in the GISS data set. This transition takes place on multidecadal timescales nearly everywhere. The red color denotes locations that do not show pink-noise characteristics on timescales up to 65 yr (half of the total length of the data set), with the most prominent feature being in the tropical eastern Pacific. White regions show locations where continuous data are absent.

evaporation, reflecting the variability in surface heat flux.

To examine the spatial structure of $d(\tau)$, and whether it captures the principal contributions to decadal variability, we construct two one-point correlation maps. As seen in Fig. 2, $d(\tau)$ nearly mirrors two key decadal variability indices: (a) the Pacific Decadal Oscillation (PDO) [6] and (b) the North Atlantic Oscillation (NAO) [29]. We use empirical orthogonal function (EOF) analysis [30] to determine the dominant spatial pattern. Figure 2(c) shows the first EOF mode and explains 21% of the total variance, with the rest of the modes characterized by shorter timescales [20]. This first mode connects the major PDO region in the eastern Pacific to the Southern Ocean region (also seen in simulations [31]) and is very similar to the so-called “hyperclimate modes” [32] and the “Interdecadal Pacific Oscillation” (IPO) [8] in the Pacific Ocean. The time series of the principal component (PC) shows clear multidecadal variability. We note that the sign of the mode changes from positive to negative at about the start of the new millennium. A negative sign denotes the intensification of the negative PDO in the North Pacific and the cooling of the Southern Ocean circumpolar region. Simulations [1,3] have shown that the cooling of the eastern tropics is correlated with the global warming hiatus, and the average sea surface temperature trends from ten climate models, which capture the hiatus, are negative in the Eastern Pacific and Southern Ocean [4]. The leading EOF of $d(\tau)$ introduced here may be related to this hiatus. Figure 2(d) shows the result of MFTW DFA using the time series of the PC; the onset of pink-noise behavior occurs after approximately 15 yr, indicated by the fluctuation function mirroring the red dashed line denoting $\beta = 1$. This noise behavior and its global presence on multidecadal timescales raises the

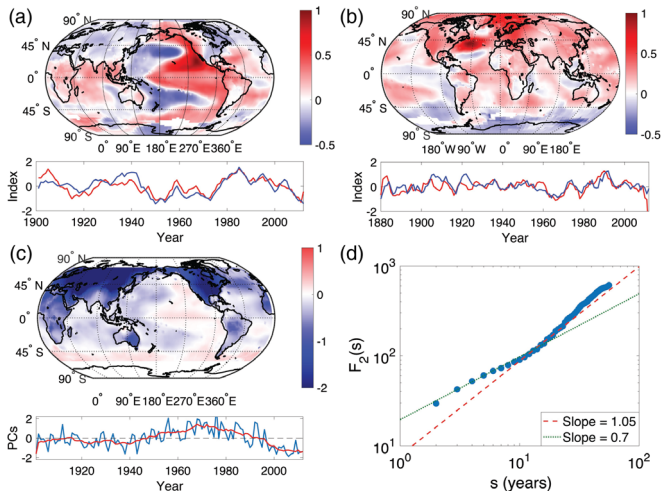


FIG. 2. Spatial distribution of the values of $d(\tau)$ represented by one-point correlation maps and an EOF analysis using the GISS monthly averaged surface temperature from 1901 to 2012. Centered in the eastern Pacific at 120°W , 20°N , we calculate the correlation between the $d(\tau)$ at this position and that at any other position (a). The spatial distribution of the correlation is nearly identical to the dipole mode called the PDO [1]. The newly constructed dipole of $d(\tau)|_{120^\circ\text{W},20^\circ\text{N}} - d(\tau)|_{180^\circ\text{E},40^\circ\text{N}}$, is compared with the traditional normalized PDO index (red), which shows an excellent match. A similar one-point correlation map is constructed based on the geographic position at 50°W , 38°N and is shown in (b). This map is very similar to the SST pattern in the negative state of the NAO [19], as shown by the correlation between $d(\tau)|_{50^\circ\text{W},38^\circ\text{N}} - d(\tau)|_{40^\circ\text{W},50^\circ\text{N}}$ (red) and the normalized NAO index (blue). The EOF analysis is applied to the values of $d(\tau)$, with the leading mode explaining 21% of the total variance, as shown in (c), along with the PC. This mode connects the major PDO region in the eastern Pacific to the Southern Ocean through a continuous same-sign region, as distinguished from the other areas. The time series of the principle component of the mode is analyzed using MFTW DFA (d). At lower frequencies, the variability of $d(\tau)$ parallels pink noise (red dashed line, $\beta = 1$), with a crossover time of ≈ 15 yr.

natural question: Is pink-noise dynamics an internal feature of the multidecadal variability of our climate or imprinted on the climate system by anthropogenic forcing? We address this question by analyzing paleoclimate proxies.

Paleoclimate studies have been broadly successful in observing the long-term evolution and variability of Earth's climate (see, e.g., [33,34]). Because of their comparatively high resolution, we focus on the proxy data from speleothems and ice cores to (a) understand the observed pink signal in the GISS data and (b) study the effect of anthropogenic climate change on natural climate variability. Our data sets cover a substantial swath of the globe: Asia, Europe, North America, Central America, South America, and Antarctica along with the Pacific Islands [20]. These data provide a long record of Earth's climate system, drawing from many sources dating back more than

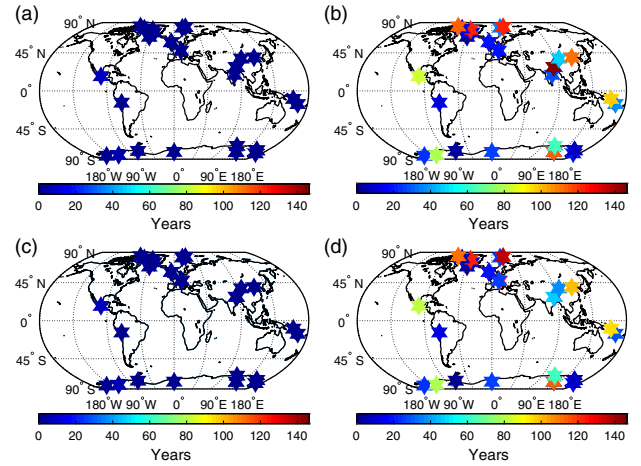


FIG. 3. The initial (a),(c) and final (b),(d) timescales exhibiting pink-noise dynamics in the paleoclimate data across the globe [20], where (a) and (b) [(c) and (d)] show the analysis for the complete data set (after removing data from 1850 to present), to enable us to distinguish between natural climate variability and anthropogenic forcing. There are no discernible differences between (a),(b) and (c),(d), implying that pink-noise dynamics are an internal characteristic of Earth's climate system.

100 000 yr. Figures 3(a,b) show the initial and final timescales exhibiting pink-noise dynamics for the paleoclimate proxy data from various sources [20]. Two things are immediately evident: Nearly all data sets show consistent pink-noise behavior, and, as was observed in the GISS data set, the transition timescale to this behavior depends on the geographic location.

To study the impact of anthropogenic forcing on internal climate variability and the observed pink-noise behavior, we use MFTW DFA to analyze only data up to 1850 A.D. Figure 3 shows that the timescales exhibiting pink-noise dynamics with and without the postindustrial period exhibit very little difference, indicating that the observed pink-noise behavior is intrinsic to Earth's climate dynamics. In data from the past 80 000 yr, we also find a timescale of approximately 1470 yr (Fig. 4), the signal often ascribed to Dansgaard-Oeschger (DO) events [34]. We hypothesize the possibility of a stochastic resonance process due to the presence of pink noise on multidecadal timescales as follows. Nozaki and Yamamoto [35] showed that for noise with $1/f^\beta$, $0 \leq \beta \leq 2$, the noise intensity for which resonance takes place is *minimized* when $\beta \approx 1$ for relaxation oscillator dynamical systems, and DO events exhibit relaxation oscillation behavior [36,37]. Thus, the resonance efficiency is *maximal* for $\beta \approx 1$, and in all of these proxies DO events are preceded by pink noise on multidecadal to centennial timescales, suggesting that a much smaller pink-noise intensity can lead to a new climatic state relative to other noise types, such as white noise. Importantly, whether the DO events arise from stochastic resonance, a “ghost resonance,” or a related process is actively debated

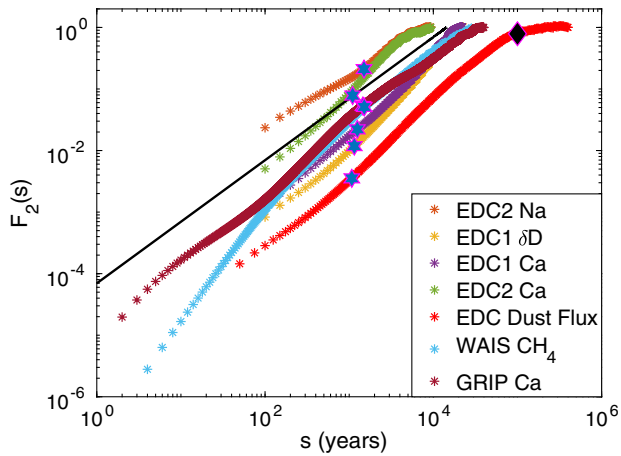


FIG. 4. Fluctuation functions $F_2(s)$ for paleoclimate proxy data (see the inset and Table I in Ref. [20]) spanning at least the past 80 000 yr. The blue stars show the crossover timescale of ~ 1470 yr, associated with Dansgaard-Oeschger events. For reference, the black diamond denotes the 100 000-yr Milankovitch eccentricity cycle, the timescale of Late Pleistocene glaciations. The black line has a slope of unity ($\beta = 1$).

(see, e.g., [37–42]), and here we emphasize that the timescale emerges from a stochastic data analysis method with no assumptions regarding periodicity. We note further that in the dust flux data, which spans the past 800 000 yr, we see a clear periodic 100 000-yr signal related to the Milankovitch eccentricity cycle, providing a fidelity check for our methodology.

Proxies such as $\delta^{18}\text{O}$ and $\delta^{13}\text{C}$, from ice cores and speleothems, are used to infer past temperature, among other climate variables. Because the temperature reflects the heat flux at a given location, such flux-dependent quantities are key mirrors of the climate system. In the low (high) latitudes, heat fluxes drive precipitation and evaporation (freezing and melting). Thus, global moisture fluxes are reflected with high fidelity in the ice core and speleothem proxy data and thereby encode aspects of climate variability. For example, the ENSO underlies major global rainfall patterns through atmospheric and oceanic teleconnections. Importantly, there are regional differences in the timescales over which the various paleoclimate proxies exhibit pink noise. Each precipitation-based proxy depends on the net heat flux at a given location, and hence we expect regional variability of the pink-noise timescales.

Analysis of sea surface temperature (SST) data has also revealed pink noise in the midlatitudes [43], rationalized by a simple vertical diffusion model with a shallow mixed layer forced by random atmospheric motions [44]. Essential here is the accumulation of the response from random atmospheric forcing due to the large heat capacity of the ocean. This local variability in the midlatitude and tropical oceans is transferred to the global scale via atmospheric teleconnections and ocean waves [28,45]. Here, this is reflected in our first EOF mode with a time

evolution that shows pink-noise statistics on multidecadal timescales. Moreover, the IPO, which we have shown mirrors our first EOF mode, is strongly linked to global precipitation [45], consistent with the relationship between the pink-noise behavior found in the proxies that reflect precipitation and the EOF mode.

Kendal and Jørgensen [13] have shown that both pink noise and fluctuation scaling [wherein the variance of a sequence of observations x is related to the mean by a power law; $\text{Var}(x) \propto \bar{x}^b$] imply each other and can be explained by a central limitlike convergence theorem that establishes which Tweedie exponential dispersion models act as foci for this convergence [46]. The duality between fluctuation scaling and pink noise provides not only a universal treatment of the statistics of the global mode that emerges from this wide range of data we have studied but a common understanding of their non-Gaussianity.

We note that the intrinsic nature of both the first EOF mode and the pink-noise behavior suggest the intriguing potential of a resonance with external low-frequency forcing, such as that associated with anthropogenic effects. Such a resonance may underlie processes associated with the global warming hiatus, emphasizing the importance of understanding internal multidecadal variability.

Finally, nonautonomous stochastic differential equations constitute a key organizing center of our approach [27], and they are also central to the so-called supersymmetric theory of stochastics (see, e.g., [47,48]). That approach argues that pink noise is a manifestation of the spontaneous breakdown of topological supersymmetry. However, to ascribe the associated Goldstone modes to specific climate processes is too speculative at present, although the breaking of time-reversal symmetry by Earth’s rotation has been shown to provide a topological origin for equatorially trapped waves [49]. Therefore, understanding the origin of the emergence of the decadal modes in the climate system that we have observed here may be fruitfully pursued along these lines.

The authors thank Peter Ditlevsen for constructive comments and criticisms. W. M. acknowledges a Herchel-Smith postdoctoral fellowship for support. S. A. acknowledges the David Crighton fellowship for support. S. A. and J. S. W. acknowledge National Aeronautics and Space Administration Grant No. NNH13ZDA001N-CRYO. J. S. W. and W. M. acknowledge Swedish Research Council Grant No. 638-2013-9243, and J. S. W. a Royal Society Wolfson Research Merit Award for support.

-
- [1] Y. Kosaka and S.-P. Xie, *Nature (London)* **501**, 403 (2013).
 - [2] T. R. Karl, A. Arguez, B. Huang, J. H. Lawrimore, J. R. McMahon, M. J. Menne, T. C. Peterson, R. S. Vose, and H.-M. Zhang, *Science* **348**, 1469 (2015).
 - [3] K. E. Trenberth and J. T. Fasullo, *Earth’s Future* **1**, 19 (2013).

- [4] M. Watanabe, H. Shiogama, H. Tatebe, M. Hayashi, M. Ishii, and M. Kimoto, *Nat. Clim. Change* **4**, 893 (2014).
- [5] G. A. Meehl, H. Teng, and J. M. Arblaster, *Nat. Clim. Change* **4**, 898 (2014).
- [6] N. J. Mantua and S. R. Hare, *J. Oceanogr.* **58**, 35 (2002).
- [7] M. E. Schlesinger and N. Ramankutty, *Nature (London)* **367**, 723 (1994).
- [8] M. J. Salinger, J. A. Renwick, and A. B. Mullan, *International Journal of Climatology* **21**, 1705 (2001).
- [9] T. P. Barnett, *Mon. Weather Rev.* **106**, 1353 (1978).
- [10] J. Ludescher, M. I. Bogachev, J. W. Kantelhardt, A. Y. Schumann, and A. Bunde, *Physica* **390A**, 2480 (2011).
- [11] S. Agarwal, W. Moon, and J. S. Wettlaufer, *Proc. R. Soc. A* **468**, 2416 (2012).
- [12] J. Davidsen and H. G. Schuster, *Phys. Rev. E* **65**, 026120 (2002).
- [13] W. S. Kendal and B. Jørgensen, *Phys. Rev. E* **84**, 066120 (2011).
- [14] R. Blender, X. Zhu, and K. Fraedrich, *Adv. Sci. Res.* **6**, 137 (2011).
- [15] M. Niemann, H. Kantz, and E. Barkai, *Phys. Rev. Lett.* **110**, 140603 (2013).
- [16] J. Hérault, F. Petrelis, and S. Fauve, *Europhys. Lett.* **111**, 44002 (2015).
- [17] M. Brownnutt, M. Kumph, P. Rabl, and R. Blatt, *Rev. Mod. Phys.* **87**, 1419 (2015).
- [18] GISTEMP-Team, GISS Surface Temperature Analysis (GISTEMP), NASA Goddard Institute for Space Studies. Data set accessed 2017-01-15.
- [19] J. Hansen, R. Ruedy, M. Sato, and K. Lo, *Rev. Geophys.* **48**, RG4004 (2010).
- [20] See Supplemental Material at <http://link.aps.org/supplemental/10.1103/PhysRevLett.121.108701> for a description of the data sets used, MFTWDFFA, statistical analysis of exponents, stochastic time-series analysis method, and the EOF method, which includes Refs. [21,22].
- [21] P. Huybers and W. Curry, *Nature (London)* **441**, 329 (2006).
- [22] Z. G. Shao and P. D. Ditlevsen, *Nat. Commun.* **7**, 10951 (2016).
- [23] Y. Zhou and Y. Leung, *J. Stat. Mech.* (2010) P06021.
- [24] S. Agarwal and J. S. Wettlaufer, *J. Clim.* **30**, 4873 (2017).
- [25] S. Agarwal, F. D. Sordo, and J. S. Wettlaufer, *Astron. J.* **153**, 12 (2017).
- [26] O. Løvsletten, *Phys. Rev. E* **96**, 012141 (2017).
- [27] W. Moon and J. S. Wettlaufer, *Sci. Rep.* **7**, 44228 (2017).
- [28] Z. Liu and M. Alexander, *Rev. Geophys.* **45**, RG2005 (2007).
- [29] H. Wanner, S. Brönnimann, C. Casty, D. Gyalistras, J. Luterbacher, C. Schmutz, D. B. Stephenson, and E. Xoplaki, *Surv. Geophys.* **22**, 321 (2001).
- [30] E. N. Lorenz, technical report, Department of Meteorology, MIT, 1956, http://eaps4.mit.edu/research/Lorenz/Empirical_Orthogonal_Functions_1956.pdf.
- [31] D. L. Bars, J. P. Viebahn, and H. A. Dijkstra, *Geophys. Res. Lett.* **43**, 2102 (2016).
- [32] D. Dommenget and M. Latif, *Geophys. Res. Lett.* **35**, L02706 (2008).
- [33] J. Zachos, M. Pagani, L. Sloan, E. Thomas, and K. Billups, *Science* **292**, 686 (2001).
- [34] W. Dansgaard, S. J. Johnsen, H. B. Clausen, D. Dahl-Jensen, N. S. Gundestrup, C. U. Hammer, C. S. Hvidberg, J. P. Steffensen, A. E. Sveinbjörnsdóttir, J. Jouzel, and G. Bond, *Nature (London)* **364**, 218 (1993).
- [35] D. Nozaki and Y. Yamamoto, *Phys. Lett. A* **243**, 281 (1998).
- [36] A. Timmermann, H. Gildor, M. Schulz, and E. Tziperman, *J. Clim.* **16**, 2569 (2003).
- [37] N. Boers, M. D. Chekroun, H. Liu, D. Kondrashov, D.-D. Rousseau, A. Svensson, M. Bigler, and M. Ghil, *Earth Syst. Dynam.* **8**, 1171 (2017).
- [38] C. Wunsch, *Paleoceanography* **15**, 417 (2000).
- [39] P. D. Ditlevsen, M. S. Kristensen, and K. K. Andersen, *J. Clim.* **18**, 2594 (2005).
- [40] P. Balenzuela, H. Braun, and D. R. Chialvo, *Contemp. Phys.* **53**, 17 (2012).
- [41] S. Krumscheid, M. Pradas, G. A. Pavliotis, and S. Kalliadasis, *Phys. Rev. E* **92**, 042139 (2015).
- [42] M. Rypdal, *J. Clim.* **29**, 4047 (2016).
- [43] K. Fraedrich and R. Blender, *Phys. Rev. Lett.* **90**, 108501 (2003).
- [44] K. Fraedrich, U. Luksch, and R. Blender, *Phys. Rev. E* **70**, 037301 (2004).
- [45] B. Dong and A. Dai, *Clim. Dyn.* **45**, 2667 (2015).
- [46] B. Jørgensen, J. R. Martinez, and M. Tsao, *Scand. J. Stat.* **21**, 223 (1994).
- [47] I. V. Ovchinnikov, *Chaos* **22**, 033134 (2012).
- [48] I. V. Ovchinnikov, *Entropy* **18**, 108 (2016).
- [49] P. Delplace, J. B. Marston, and A. Venaille, *Science* **358**, 1075 (2017).